Journal of Power Sources 244 (2013) 87–93

Contents lists available at SciVerse ScienceDirect

Journal of Power Sources

journal homepage: www.elsevier.com/locate/jpowsour

New fluorophosphate $Li_{2-x}Na_xFe[PO_4]F$ as cathode material for lithium ion battery

Hamdi Ben Yahia*, Masahiro Shikano*, Shinji Koike, Hikari Sakaebe, Mitsuharu Tabuchi, Hironori Kobayashi

Research Institute for Ubiquitous Energy Devices, National Institute of Advanced Industrial Science and Technology (AIST), 1-8-31 Midorigaoka, Ikeda, Osaka 563-8577, Japan

HIGHLIGHTS

- $Li_2Fe[PO_4]F$ was prepared from $LiNaFe[PO_4]F$ by ion exchange using LiBr in ethanol.
- $Li_2Fe[PO_4]F$ and $LiNaFe[PO_4]F$ crystallize with the $Li_2Ni[PO_4]F$-type structure.
- It is different from the Tavorite $Li_{1+x}Fe[PO_4]F$- and the layered $Na_2Fe[PO_4]F$-type.
- ^{57}Fe Mössbauer were collected at different stages of the galvanometric cycling.
- Up to 1 mol of alkali metal is extractable between 1.0 V and 5.1 V *vs.* Li^+/Li.

GRAPHICAL ABSTRACT

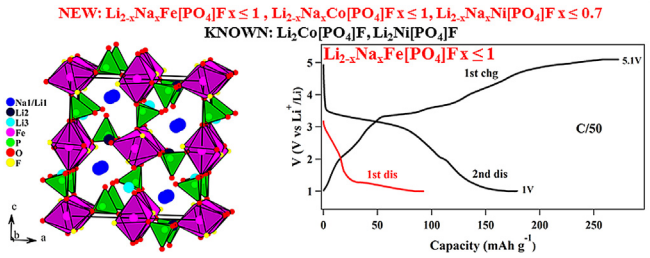

ARTICLE INFO

Article history:
Received 18 September 2012
Received in revised form
22 March 2013
Accepted 23 March 2013
Available online 3 April 2013

Keywords:
Fluorophosphate
Ion Exchange
Mössbauer spectroscopy
Positive electrode
Lithium ion battery

ABSTRACT

The new compound $Li_{1.65}Na_{0.35}Fe[PO_4]F$ with the $Li_2Ni[PO_4]F$ structure has been prepared from the analogous $LiNaFe[PO_4]F$ phase by ion exchange using LiBr in ethanol at 90 °C. The sample was characterized by powder X-ray diffraction, ^{57}Fe Mössbauer spectroscopy, and electrochemical measurements. $Li_{1.65}Na_{0.35}Fe[PO_4]F$ crystallizes with orthorhombic symmetry, space group *Pnma*, with $a = 10.5093(5)$ Å, $b = 6.4999(2)$ Å, $c = 11.0483(5)$ Å, $V = 754.70(7)$ Å^3, and $Z = 8$. The ^{57}Fe Mössbauer data collected at different stages of galvanometric cycling confirmed that only 1 mol of alkali metal is extractable between 1.0 V and 5.1 V *vs.* Li^+/Li with a discharge capacity between 135 and 145 mA h g^{-1}. Li/Na electrochemical ion exchange occurs during cycling and leads to a lithium rich phase.

© 2013 Elsevier B.V. All rights reserved.

1. Introduction

For a material to be successfully used as a positive electrode in a rechargeable lithium battery, it is necessary that it has a stable structure during charge and discharge, has a high ionic and electric conductivity, has a high energy density and contains preferably low cost and environmentally benign components. Moreover, for the

* Corresponding authors. Tel.: +81 72 751 7932; fax: +81 72 751 9609.
E-mail addresses: benyahia.hamdi@voila.fr, benyahia.hamdi@aist.go.jp (H. Ben Yahia), shikano.masahiro@aist.go.jp (M. Shikano).

0378-7753/$ – see front matter © 2013 Elsevier B.V. All rights reserved.
http://dx.doi.org/10.1016/j.jpowsour.2013.03.128

large-scale batteries for hybrid electric vehicles, the safety of the system needs to be considered [1]. Based on these requirements, an improvement of the electrochemical properties and safety of the existing materials such as the ABO_2 layered oxides (e.g., $LiNi_{1/3}Mn_{1/3}Co_{1/3}O_2$ and $LiNi_{1-x-y}Co_xAl_yO_2$) with α-$NaFeO_2$-type structure is needed. Thus, various techniques such as cation and/or anion substitution, coating, etc. have been used [2]. In addition, there is a need to explore new systems to discover new materials as in the case of polyanion (XO_4^{y-}: X = P, Si)-based materials that have been extensively studied as positive electrode materials in lithium ion batteries. The olivine $LiFePO_4$ (theoretical capacity = 170 mA h g^{-1}) is a particularly promising example due to its advantages of being environmentally benign, inexpensive and safe [3]. However, there is a need for a higher energy density that could be achieved by increasing the capacity and the discharge voltage.

Attempts have been made to expand the capacity by using materials such as Li_2FeSiO_4 (theoretical capacity = 331 mA h g^{-1}), which theoretically could extract two lithium atoms per formula unit. Higher discharge capacities than $LiFePO_4$ have been observed in these silicates [4]. Few other researchers have focused their studies on the $A_2M[PO_4]F$ fluorophosphates. Indeed, Okada et al. have studied the electrochemical properties of $Li_2Co[PO_4]F$ and $Li_2Ni[PO_4]F$ [5,6]. Nazar et al. have studied $Li_2Fe[PO_4]F$ (theoretical capacity = 292 mA h g^{-1}) to find that the intercalation of one Li atom into $LiFe[PO_4]F$ (tavorite structure) is possible with a reversible and stable capacity of 145 mA h g^{-1} around a potential of 3 V [7]. Nazar and Yang research groups have also synthesized $Na_{2-x}Li_xM[PO_4]F$ by different ion exchange methods starting from layered structure of $Na_2M[PO_4]F$ (M = Fe, Co, Mg) [8,9]. Nazar et al. have also synthesized $Na_2Ni[PO_4]F$ and suggested that it is isostructural with $Na_2Fe[PO_4]F$ [10]. However, we demonstrated recently that Na_2NiPO_4F crystallizes with a new type of structure different from $Na_2M[PO_4]F$ (M: Fe, Co, Mg) [11]. Furthermore, we have shown that $LiNaCo[PO_4]F$ and $LiNaFe[PO_4]F$ exist and crystallize with the $Li_2Ni[PO_4]F$-type [12,13].

In the present work we synthesized the $Li_{1.65}Na_{0.35}Fe[PO_4]F$ compound, solved its crystal structure using powder X-ray diffraction data, and characterized its properties by ^{57}Fe Mössbauer spectroscopy, and electrochemical measurements. Results of our study are described in the following.

2. Experimental section

2.1. Synthesis

Powder sample of $LiNaFe[PO_4]F$ was prepared by direct solid state reaction from stoichiometric mixture of NaF and $LiFePO_4$. The mixture was ball milled in ethanol for 6 h in a planetary ball mill (600 rpm). The mixed slurry was then dried, pelletized and fired at 600 °C for 10 h in a platinum crucible under argon flow. The progress of the reaction was followed by powder X-ray diffraction and no impurities have been observed in this sample. 1 g of $LiNaFe[PO_4]F$ and 10 g of LiBr were then placed in 100 cm^3 of ethanol. The mixture was refluxed at 90 °C for 48 h, with continuous stirring. The product was filtered, washed and dried. This led to the new phase $Li_{1.65}Na_{0.35}Fe[PO_4]F$.

2.2. Elemental analyses

Semiquantitative EDX analyses of the $Li_{1.65}Na_{0.35}Fe[PO_4]F$ electrode (Fig. S1) was carried out with a JSM-500LV (JEOL) scanning electron microscope. The experimentally observed composition (Na/Fe/P) was (0.32:0.97:1) at the initial stage and (0.09:0.83:1) after the 51st cycle. The resolution of the machine did not allow a reliable determination of the lithium, fluorine and oxygen content. The presence of sodium atoms has been confirmed by ICP analysis which revealed a Na/Li/Fe/P molar ratio of 0.40:1.68:0.95:1 for the initial phase. This indicates that the Li/Na ion exchange was not total.

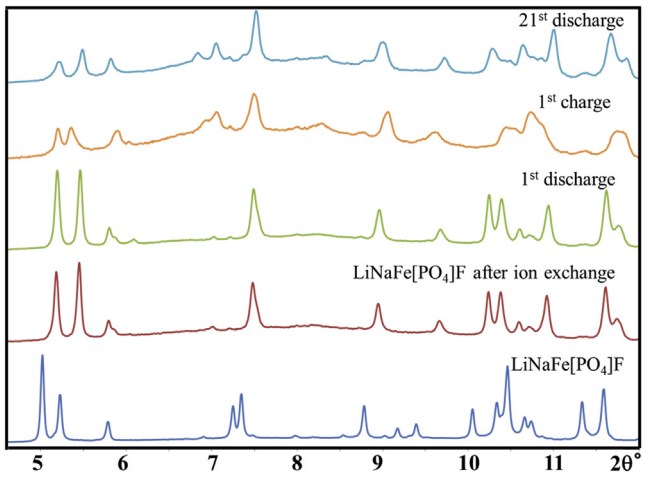

Fig. 1. Synchrotron X-ray powder diffraction patterns (λ = 0.5003 Å) of $LiNaFe[PO_4]F$ before and after ion exchange, and $Li_{1.65}Na_{0.35}Fe[PO_4]F$ after the 1st discharge to 1.0 V, the 1st charge to 5.0 V, and the 21st discharge to 1.0 V.

2.3. X-ray diffraction

To check the purity of the powders, high resolution X-ray powder diffraction measurements were performed (Fig. S2, S3). The data were collected at room temperature over the 2θ angle range $10° \leq 2\theta \leq 80°$ with a step size of 0.01° using a Rigaku diffractometer operating with Cu$K\alpha$1,α2 radiations. Full pattern matching refinements were performed with the JANA2006 program package [14]. The backgrounds were estimated by a Legendre function, and the peak shapes were described by a pseudo-Voigt function.

High resolution X-Ray powder diffraction data, using synchrotron radiation (λ = 0.5003 Å), have been also collected on BL19B2 at SPring-8 (with the approval of the Japan Synchrotron Radiation Research Institute (Proposal No. 2011A1795)) for $LiNaFe[PO_4]F$, $Li_{1.65}Na_{0.35}Fe[PO_4]F$, and for $Li_{1.65}Na_{0.35}Fe[PO_4]F$ after the 1st discharge, the 1st charge and the 21st discharge (Fig. 1). The determined cell parameters are listed in Table 1.

2.4. ^{57}Fe Mössbauer spectroscopy

To check the purity of the $Li_{1.65}Na_{0.35}Fe[PO_4]F$ powder, the ^{57}Fe Mössbauer spectra were collected with a ^{57}Co γ-ray source. The

Table 1
Evolution of the cell parameters of $LiNaFe[PO_4]F$ after ion exchange and during the galvanometric cycling.

Samples	a (Å)	b (Å)	c (Å)	V (Å^3)
$LiNaFe[PO_4]F$	10.9739(1)	6.3589(5)	11.4237(1)	797.17(6)
$Li_{1.65}Na_{0.35}Fe[PO_4]F$ (obtained by ion exchange)	10.5093(5)	6.4999(2)	11.0483(5)	754.70(7)
$Li_{1.65}Na_{0.35}Fe[PO_4]F$ after the 1st discharge	10.5069(1)	6.50425(8)	11.0486(1)	755.06(1)
$Li_{1.65}Na_{0.35}Fe[PO_4]F$ after the 1st charge	10.6162(17)	6.3970(8)	10.8985(13)	740.2(2)
$Li_{1.65}Na_{0.35}Fe[PO_4]F$ after the 21st discharge	10.4465(4)	6.4815(4)	10.9805(7)	743.48(6)

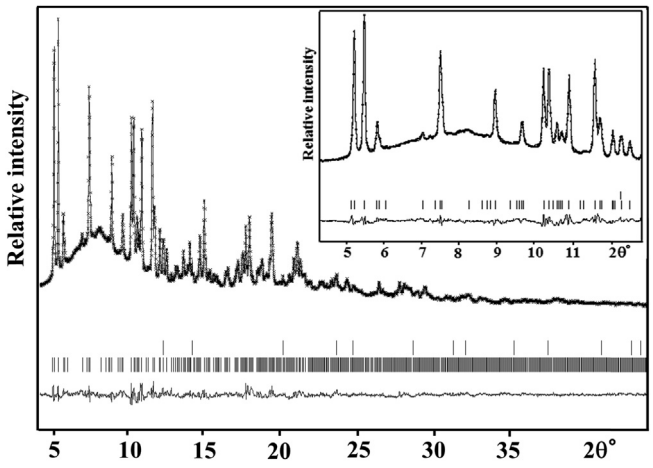

Fig. 2. Rietveld plot for $Li_{1.65}Na_{0.35}Fe[PO_4]F$-synchrotron powder diffraction data at 293 K ($\lambda = 0.5003$ Å). The tick marks indicate the peaks of LiF (top) and $Li_{1.65}Na_{0.35}Fe[PO_4]F$ (bottom). The inset corresponds to a zoom of the $2\theta = 4°–13°$ area.

velocity calibration was done at room temperature with a high purity α-Fe absorber. The experimental data were fitted to two symmetric doublets consisting of Lorentzian lines by using a computer program Mosswin 3.0. The isomeric shift values are given relative to that of α-Fe at room temperature.

2.5. Electrochemical cycling

Positive electrodes were made from mixtures of $Li_{1.65}Na_{0.35}Fe[PO_4]F$ powder, acetylene black (AB) and polyvinylidene fluoride (PVDF) binder dissolved in N-methylpyrrolidone in a weight ratio of 70:22:8. The obtained slurry was mixed for 1 h, and coated onto an Al foil. The resulting electrode films were pressed with a twin roller, cut into a round plate ($\Phi = 14$ mm) and dried at 110 °C for 24 h under vacuum. $Li_{1.65}Na_{0.35}Fe[PO_4]F/LiPF_6$+EC + DMC/Li coin-type cell (CR2032) and laminated cell were assembled, in an argon-filled glove box, with polypropylene as separator. CC–CV test was performed using BTS2003H (Nagano Co., Ltd) battery tester system in a potential range of 1.0–4.4 V, 1.0–5.0 V at a rate of C/5 and also in the range 1.0–5.1 V at a rate of C/50 (that is, one lithium per formula unit in 50 h).

Table 2
Crystallographic data and structure refinement for $Li_{1.65}Na_{0.35}Fe[PO_4]F$.

Rietveld refinement	
Crystal data	
Phase 1: $Li_{1.65}Na_{0.35}Fe[PO_4]F$	$V = 754.93(5)$ Å^3
$M_r = 189.5$	$Z = 8$
Orthorhombic, *Pnma*	$D_x = 3.333$ Mg m^{-3}
$a = 10.5108(4)$ Å	synchrotron, $\lambda = 0.5003$ Å
$b = 6.4996(2)$ Å	$T = 300$ K
$c = 11.0504(5)$ Å	beige
Phase 2: LiF	$V = 66.33$ (1) Å^3
$M_r = 25.94$	$a = 4.0479$ (3) Å
Cubic, Fm-3m	$Z = 4$
Data collection	
BL19B2 diffractometer at Spring-8	
$2\theta_{min} = 0.01°$, $2\theta_{max} = 78.01°$, $2\theta_{step} = 0.01°$	
Refinement	
$R_p = 0.0254$	41 parameters
$R_{wp} = 0.0334$	7801 data points
$R_B = 0.0938$	Profile function: Pseudo-Voigt
$\chi^2 = 0.87$	Background: manual
Excluded regions: from 0 to 4 and from 44 to 78.01	

Table 3
Atom positions for $Li_{1.65}Na_{0.35}Fe[PO_4]F$ from the synchrotron powder diffraction data at 293 K. The isotopic displacement parameters are equal to 0.0184(3) Å^2.

Atom	Wyck.	Occ.	*x*	*y*	*z*
Fe1	4*a*	1	0	0	0
Fe2	4*b*	1	0	0	1/2
P1	4*c*	1	0.0074(11)	1/4	0.7493(12)
P2	4*c*	1	0.2443(11)	1/4	0.0885(8)
Na1	8*d*	0.35	0.2655(15)	0.002(3)	0.3351(8)
Li1	8*d*	0.65	0.2655(15)	0.002(3)	0.3351(8)
Li2	4*c*	1	0.535	1/4	0.2078
Li3	4*c*	1	0.253(6)	1/4	0.590(5)
O1	8*d*	1	0.1910(8)	0.0668(13)	0.0242(8)
O2	4*c*	1	0.2007(13)	1/4	0.2346(16)
O3	4*c*	1	0.1639(15)	1/4	0.7290(15)
O4	4*c*	1	0.3843(14)	1/4	0.0593(13)
O5	4*c*	1	0.4705(18)	1/4	0.6231(16)
O6	8*d*	1	0.0312(9)	0.5570(16)	0.3258(7)
F1	4*c*	1	0.1324(11)	1/4	0.4679(11)
F2	4*c*	1	0.4386(13)	1/4	0.3806(11)

3. Results and discussion

3.1. Structure refinement

The structure of $Li_{1.65}Na_{0.35}Fe[PO_4]F$ was solved using the crystal structure of $LiNaFe[PO_4]F$ as starting model [13]. By introducing a Li/Na statistical disorder on the sodium crystallographic site, the Rietveld analysis of the synchrotron powder diffraction data collected at 293 K led to low reliability factors, however few atoms had negative isotropic displacement parameters (IDP) and few peaks at $2\theta = 12.29°$ and 14.20° could not be indexed (these peaks have been attributed to the LiF impurity). By including LiF as a second phase and constraining all the atoms to have the same IDP, the reliability factors decreased to $Rp = 2.54\%$, $wRp = 3.34\%$, and $R_B = 9.38\%$ ($\chi^2 = 0.87$). The amount of LiF was estimated to 3.6(3) wt%. Fig. 2 shows a good agreement between the experimental and calculated patterns. The crystallographic data for $Li_{1.65}Na_{0.35}Fe[PO_4]F$ are listed in Table 2. The final atomic positions are given in Table 3.

3.2. Crystal structure

The analysis of the powder patterns of $LiNaFe[PO_4]F$ before and after ion exchange revealed the refined cell parameters $a = 10.9651(4)$ Å, $b = 6.3780(3)$ Å, $c = 11.4261(4)$ Å, and $V = 799.09(4)$ Å^3, and $a = 10.5249(3)$ Å, $b = 6.5093(3)$ Å,

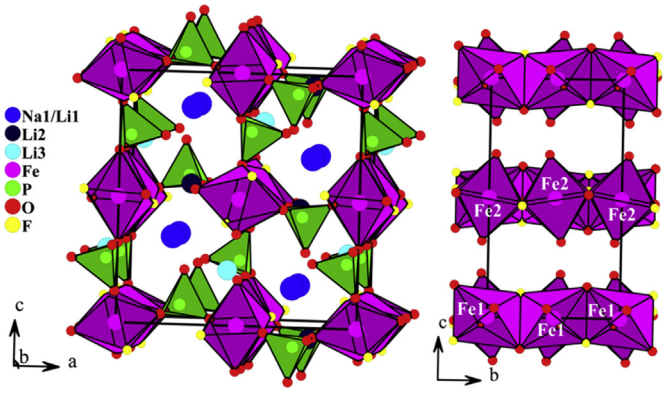

Fig. 3. Perspective view of the $Li_{1.65}Na_{0.35}Fe[PO_4]F$ structure (a), and view along [100] (b) without the phosphorus and alkali metal atoms for clarity reasons.

Table 4
Interatomic distances (in Å) and bond valences (B.V.) for $Li_{1.65}Na_{0.35}Fe[PO_4]F$. Average distances are given in brackets.

	Distance		Distance
Fe1-O1 (×2)	2.072(8)	Li1/Na1-O2	2.073(19)
Fe1-O5 (×2)	2.141(11)	Li1/Na1-O3	2.145(19)
Fe1-F2 (×2)	2.190(8)	Li1/Na1-O1	2.185(13)
	<2.134>	Li1/Na1-F2	2.494(19)
	1.93(2)[a]	Li1/Na1-O6	2.48(2)
Fe2-O6 (×2)	1.988(8)		<2.275>
Fe2-O4 (×2)	2.133(10)	Li2-O2	1.854(14)
Fe2-F1 (×2)	2.168(8)	Li2-O6 (×2)	2.030(10)
	<2.096>	Li2-F2	2.162(12)
	2.18(2)[a]	Li2-F1	2.195(12)
P1-O5	1.46(2)	Li2-O4	2.280(15)
P1-O6 (×2)	1.558(12)		<2.092>
P1-O3	1.66(2)		1.115(17)[a]
	<1.559>	Li3-O3	1.80(6)
	4.76(11)[a]	Li3-F1	1.86(6)
P2-O1 (×2)	1.495(11)	Li3-O1 (×2)	2.26(3)
P2-O2	1.68(2)	Li3-O5	2.31(7)
P2-O4	1.507(19)		<2.098>
	<1.544>		1.00(8)[a]
	4.97(10)[a]		

[a] bond valence sum, B.V. = $e^{(r0-r)/b}$ with the following parameters: $b = 0.37$, r_0 (Na^I-O) = 1.803, r_0 (Na^I-F) = 1.677, r_0 (Li^I-O) = 1.466, r_0 (Li^I-F) = 1.360, r_0 (Fe^{II}-O) = 1.734, r_0 (Fe^{II}-F) = 1.658 and r_0 (P^V-O) = 1.617 Å [16,17].

$c = 11.0481(4)$ Å, and $V = 756.91(4)$ Å^3 for $LiNaFe[PO_4]F$ and $Li_{1.65}Na_{0.35}Fe[PO_4]F$, respectively. The significant decrease of the cell volume indicates that the ion exchange of Na^+ by Li^+ ions clearly occurred but was not total. The refined Li/Na molar ratio of 0.64:0.36 (Table 3) is in very good agreement with the EDX and ICP analyses.

$Li_{1.65}Na_{0.35}Fe[PO_4]F$ is isostructural with $Li_2Ni[PO_4]F$ [15]. The structure consists of edge-sharing chains of FeF_2O_4 octahedra running along the *b* axis (Fig. 3). The $FeFO_3$ infinite chains are cross connected by the PO_4 tetrahedra, giving rise to channels and cavities in which the lithium atoms are located. One should mention that the Na/Li disorder is observed only in the channels along the *b* axis. The interatomic distances and the bond valence sums (BVSs) are listed in Table 4.

The remaining sodium atom that could not be exchanged plays an important role in stabilizing the $Li_2Ni[PO_4]F$-type structure. Indeed, when Ni is replaced by Fe, the cell volume increases significantly and the width of the channels along the *b* axis becomes too large for the lithium atoms. This explains why all the attempts to synthesize $Li_2Fe[PO_4]F$ and $Li_2Mn[PO_4]F$ by conventional synthesis method failed. To get the lithium rich phase $A_2M[PO_4]F$ (*M*: Fe, Mn) crystallizing with the $Li_2Ni[PO_4]F$-type structure, it is necessary to dope the *A* sites with sodium or attempt to decrease the cell volume by doping the *M* sites with a smaller transition metal.

3.3. ^{57}Fe Mössbauer spectroscopy of $Li_{1.65}Na_{0.35}Fe[PO_4]F$

The ^{57}Fe Mössbauer spectra of $Li_{1.65}Na_{0.35}Fe[PO_4]F$, measured at room temperature, during the galvanometric cycling are given in Fig. 4. In order to explain the experimental spectrum, it was necessary to consider two distributions corresponding to divalent and/or trivalent iron atoms in octahedral environments. The characteristic parameters deduced from this refinement, the isomeric shift (δ), the full width at half maximum (Γ), and quadruple splitting (Δ), are given in Table 5.

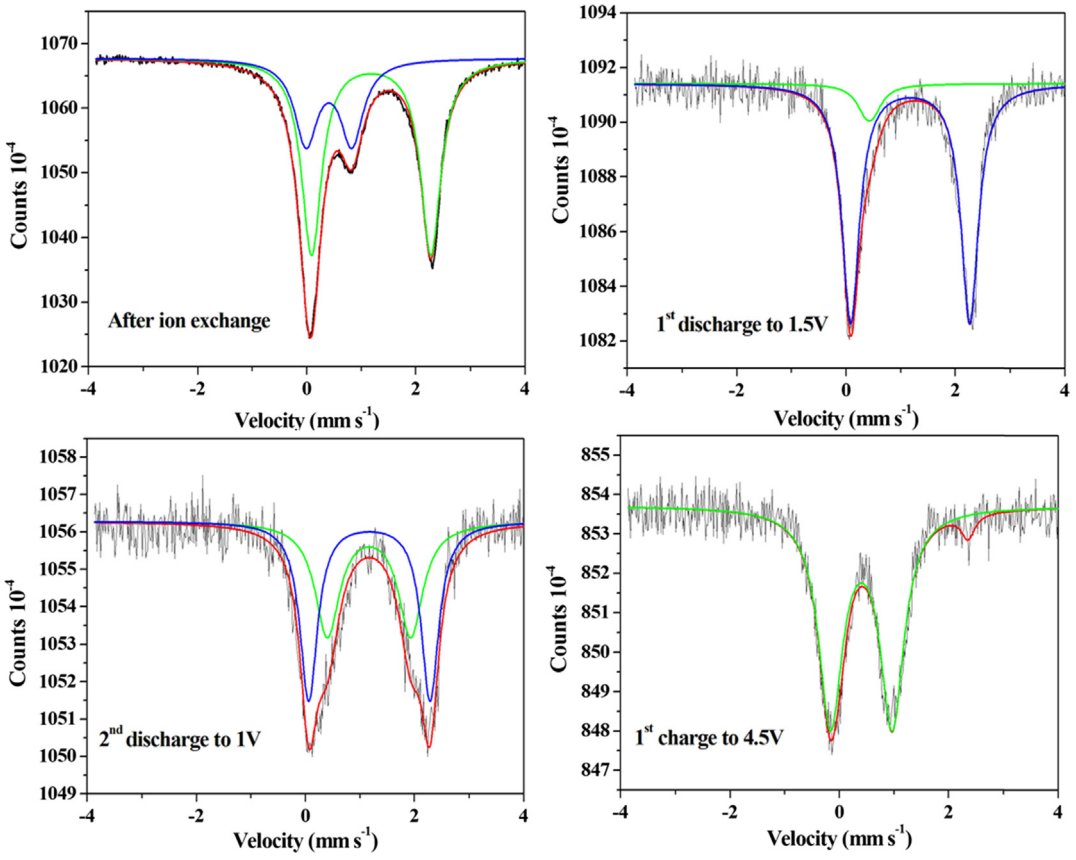

Fig. 4. The Mössbauer spectra of $Li_{1.65}Na_{0.35}Fe[PO_4]F$ during the galvanometric cycling at RT.

Table 5
Fitted Mössbauer parameters obtained for $Li_{1.65}Na_{0.35}Fe[PO_4]F$ phase (*Dis*: distribution δ = isomeric shift, Γ = full width at half maximum, and Δ = quadripole splitting).

Sample	*Dis*	δ mm s^{-1}	Γ/mm s^{-1}	Δ/mm s^{-1}	%	Site
$LiNaFe[PO_4]F$	1	1.2124(8)	0.473(2)	2.287(2)	75.7	Fe^{2+} [O_h]
Initial phase	2	0.448(3)	0.542(8)	0.729(6)	24.3	Fe^{3+} [O_h]
$Li_{1.65}Na_{0.35}Fe[PO_4]F$	1	1.162(3)	0.353(10)	2.233(6)	78.0	Fe^{2+} [O_h]
Initial phase	2	0.538(13)	0.37(3)	0.59(2)	22.0	Fe^{3+} [O_h]
$Li_{1.65}Na_{0.35}Fe[PO_4]F$	1	1.178(2)	0.384(6)	2.178(5)	91.2	Fe^{2+} [O_h]
after the 1st discharge to 1.5 V	2	0.43(2)	0.44(16)	0.13(21)	8.8	Fe^{3+} [O_h]
$Li_{1.65}Na_{0.35}Fe[PO_4]F$	1	0.405(3)	0.529(8)	1.127(6)	93.9	Fe^{3+} [O_h]
after the 1st charge to 4.5 V	2	1.199(16)	0.3	2.32(3)	6.1	Fe^{2+} [O_h]
$Li_{1.65}Na_{0.35}Fe[PO_4]F$	1	1.170(6)	0.55(2)	1.53(3)	47.0	Fe^{2+} [O_h]
after the 2nd discharge to 1.0 V	2	1.176(3)	0.391(17)	2.227(14)	53.0	Fe^{2+} [O_h]

The spectrum of $Li_{1.65}Na_{0.35}Fe[PO_4]F$ exhibits two doublets with isomeric shifts of 1.162(3) mm s^{-1} and 0.538(13) mm s^{-1} and corresponding to Fe^{2+} and Fe^{3+} in octahedral sites, respectively [18,19]. These isomeric shifts are different from those of $LiNaFe[PO_4]F$ (1.2124(8) mm s^{-1} and 0.448(3) mm s^{-1}) which indicates a distortion of the iron's octahedral sites, induced by the replacement of Na^+ by Li^+ during the ion exchange in LiBr salt. The calculated Fe^{2+}/Fe^{3+} ratio of 78/22 is very close to 75.7/24.3, calculated for the initial phase $LiNaFe[PO_4]F$. Similar to $LiNaFe[PO_4]F$, the real chemical formula of $Li_{1.65}Na_{0.35}Fe[PO_4]F$ would be $Li_{1.65}Na_{0.35}[Fe^{2+}{}_{1-x}Fe^{3+}{}_x][PO_4][F_{1-x}O_x]$ ($x \sim 1/4$) [13].

After the first discharge to 1.5 V, the contribution of Fe^{3+} decreased significantly, indicating that the structure is flexible and able to accommodate additional Li atoms. However, since the amount of Fe^{3+} is estimated to be $x \sim 1/4$, one may not be able to intercalate more than $\sim$0.25 Li^+ in the structure. In order to reduce all the Fe^{3+} ions, it is necessary to discharge the cell to 1.0 V.

As expected, during the first charge to 4.5 V, oxidation of the Fe^{2+} to Fe^{3+} is observed. The spectrum exhibits two doublets with isomeric shifts of 1.199(16) and 0.405(3) mm s^{-1}, typical values for Fe^{2+} and Fe^{3+} in octahedral sites, respectively. The calculated Fe^{2+}/Fe^{3+} ratio of 6.1/93.9 indicates that less than one alkali metal A^+ (A: Li, Na) have been deintercalated. Therefore, a higher cut-off voltage should be applied in order to extract at least one A^+ ion.

The second discharge to 1.0 V, induces a reduction of all the Fe^{3+} to Fe^{2+}. However, the spectrum is much different from the one after the first discharge. Indeed, the spectrum exhibits two doublets with quadripole splittings of 1.53(3) mm s^{-1} and 2.227(14) mm s^{-1} which confirm the presence of two different octahedral sites for divalent iron atoms Fe1 and Fe2. This is also supported by estimated Fe1/Fe2 ratio of 47/53 which is close to the theoretical value 50/50.

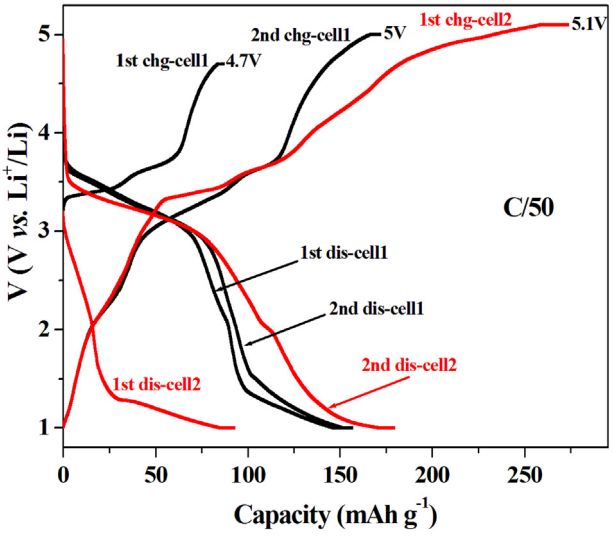

Fig. 5. Discharge/Charge curves of $Li_{1.65}Na_{0.35}Fe[PO_4]F$ recorded at RT. The cell1 was first charged to 4.7 V, whereas the cell2 was first discharged to 1 V, in a CC–CV mode (C/50).

3.4. Electrochemical properties

3.4.1. The samples discharged first to 1 V (cell2)

The discharge–charge curves of $Li_{1.65}Na_{0.35}Fe[PO_4]F$, recorded at a rate of C/50 are depicted on Fig. 5. When discharged to 1.0 V *vs.* Li^+/Li, $Li_{1.65}Na_{0.35}Fe[PO_4]F$ delivers a discharge capacity of ca. 92 mA h g^{-1}. This capacity is most probably the result of three contributions (intercalation of lithium in $Li_{1.65}Na_{0.35}Fe[PO_4]F$ and AB, and a third contribution up to now, not well explained) [20]. Only $\sim$0.25 Li^+ is expected to be intercalated in $Li_{1.65}Na_{0.35}Fe[PO_4]F$. Indeed, as mentioned in Section 3.2, there is approximately $0.25Fe^{3+}$ in the starting material $Li_{1.65}Na_{0.35}[Fe^{2+}{}_{1-x}Fe^{3+}{}_x][PO_4][F_{1-x}O_x]$ ($x \sim 1/4$), which could be reduced during the first discharge, leading to the lithium rich phase $[A_{2+x}]Fe^{2+}[PO_4][F_{1-x}O_x]$ ($x \sim 1/4$). The analysis of the ^{57}Fe Mössbauer spectra after the first discharge to 1 V confirms the presence of only Fe^{2+}in the structure. This transformation should induce a slight increase of the cell parameters, since the ionic radius of Fe^{2+} (0.78 Å) is larger than Fe^{3+} (0.645 Å). However, the analysis of the powder patterns does not show any changes of the cell parameters (Table 1). Only the intensity of the (002) reflection increased slightly. Further studies by neutron diffraction have to be carried out in order to solve accurately the crystal structure after the first discharge and determine the mechanism of Li intercalation at low voltage (1 V).

After the first charge to 5.1 V *vs.* Li^+/Li, $[A_{2+x}]Fe^{2+}[PO_4][F_{1-x}O_x]$ ($x \sim 1/4$) delivers a charge capacity above 273 mA h g^{-1}, which corresponds to the extraction of $\sim 2A^+$ ions (A = Li, Na). The analysis of the Mössbauer spectra indicates the presence of only Fe^{3+}

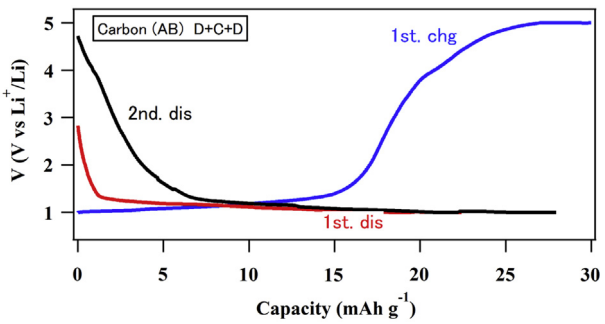

Fig. 6. Discharge/Charge curves of Li/Acetylene Black cell, recorded at room temperature, between 1.0 V and 5.0 V *vs* Li^+/Li, in a CC–CV mode (C/5).

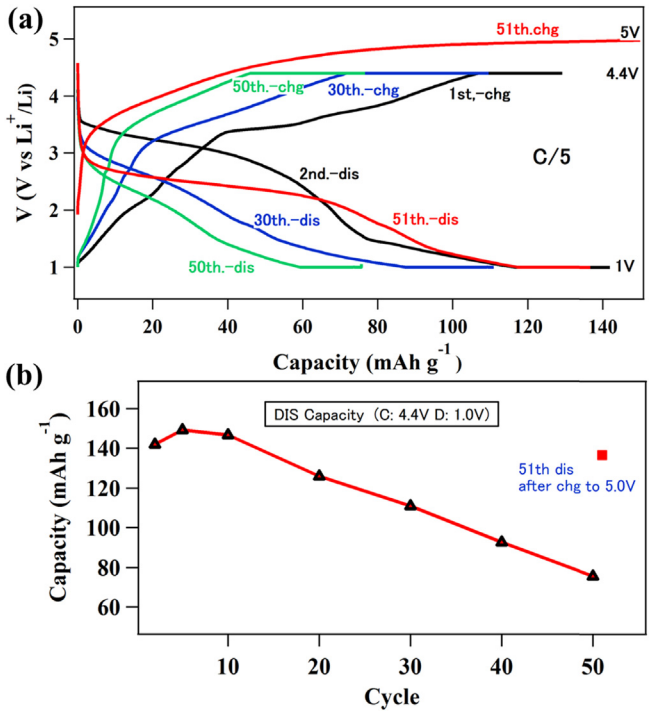

Fig. 7. Discharge/Charge curves of $Li_{1.65}Na_{0.35}Fe[PO_4]F$ recorded at room temperature, between 1.0 V and 4.4 V *vs.* Li^+/Li, in a CC–CV mode (C/5) (a), and discharge capacity retention (b). The last cycle is recorded between 1.0 V and 5.0 V after a rest time of 12 h.

(No traces of Fe^{4+} have been detected). This implies that only one alkali metal ion has been extracted from $[A_{2+x}]Fe^{2+}[PO_4][F_{1-x}O_x]$, which leads to the $[A_{1+x}]Fe^{3+}[PO_4][F_{1-x}O_x]$ (A = Li, Na and $x \sim 1/4$) composition. The additional contribution comes most probably from both, the Li intercalated in AB and the electrolyte decomposition. The intercalation of Li in AB has been confirmed using a Li/AB cell (Fig. 6).

After the second discharge to 1.0 V, a discharge capacity of 179 mA h g^{-1} has been obtained. It corresponds to the intercalation of ~1.26 alkali metal ion. Since the iron is divalent, it is concluded that only one alkali metal ion is intercalated in $[A_{1+x}]Fe^{3+}[PO_4][F_{1-x}O_x]$ (A = Li, Na and $x \sim 1/4$).

When the sample is cycled between 1.0 V and 4.4 V at a rate of C/5, the charge and discharge capacities decrease significantly (Fig. 7). This capacity fade is continuous until the 50th cycle. This is due to the shift of the charge curves to a higher voltage during cycling (Fig. 7a) which is most probably related to the replacement of the sodium- by lithium atoms. This is supported by the X-ray diffraction which shows a decrease of the unit cell volume during cycling (755.06(1) $Å^3$ and 743.48(6) $Å^3$ after the 1st and 21st discharge, respectively) due to the replacement of sodium (r_i = 1.02 Å for C.N. = 6) by lithium (r_i = 0.76 Å) atoms. Furthermore, the EDX analysis indicates a decrease of the Na/P ratio after 51cycles from 0.32/1 to 0.09/1 (Fig. S1) which is in good agreement with the occurrence of a Li/Na electrochemical ion exchange. After several cycles, this ion exchange leads to the lithium rich phase $Li_{2+x}Fe[PO_4][F_{1-x}O_x]$ ($x \sim 1/4$).

In order to avoid the decrease of the capacity during cycling it is necessary to apply a higher cut-off voltage. Indeed, when the cell is charged to 5.0 V then discharged to 1.0 V, after 50 cycles (1.0–4.4 V), a clear increase of the discharge capacity is observed (Fig. 7b). Therefore, there is a need for a stable electrolyte up to 5 V *vs.* Li^+/Li in order to extract at least one Li per unit formula. It is also important to mention that the discharge capacity values reported on Fig. 7b contain some contributions from the lithium intercalated in AB and from an additional phenomena not well understood.

3.4.2. *The samples charged first (Cell1)*

In order to avoid the decomposition of the electrolyte, the cell1 was first charged to 4.7 V. Consequently, the first discharge capacity was lower than the 2nd discharge capacity of cell2, which has been first discharged to 1 V. Therefore, during the second cycle, the cell1 was cycled between 1 and 5 V. This did not induce a significant improvement. The discharge–charge curves recorded at a rate of C/50 are depicted on Fig. 5. One clearly sees a significant difference between the cell1 (charged first) and cell2 (discharged first), especially above 3.7 V during the charge process and below 3 V during the discharge process. The charge and discharge curves are similar below 3.7 V and above 3 V, respectively. This indicates that the mechanism of intercalation and deintercalation in both cells are similar, at the beginning of each process. This is not surprising, since both materials have the same crystal structure. Perhaps the difference is due to a different arrangement of the sodium and lithium atoms in the tunnels along the *b* axis.

At 1.3 V, the compounds $Li_{1.65}Na_{0.35}Fe[PO_4]F$ (discharged first-cell2), $Li_{1.65}Na_{0.35}Fe[PO_4]F$ (charged first-cell1), and $LiNaFe[PO_4]F$ (discharged first-cell3) provide a 2nd discharge capacity of 134, 116, and 120 mA h g^{-1}, respectively, indicating that $Li_{1.65}Na_{0.35}Fe[PO_4]F$ has the best performances when discharged first (Fig. S4). When the cell with the lowest discharge capacity [$Li_{1.65}Na_{0.35}Fe[PO_4]F$ charged first-cell1 (Fig. S4)] is cycled between 1.3 V and 4.7 V at a rate of C/50 (Fig. S5), it delivers a discharge capacity of 100 mA h g^{-1} at 1.3 V and when it is charged from 1.3 V to 5.1 V, during the last cycle, a clear increase of the charge capacity is observed. Consequently, the last discharge capacity increases to 116 mA h g^{-1} at 1.3 V. This increase of 16 mA h g^{-1} indicates that more lithium has been extracted above 4.7 V and confirms that our samples have to be cycled between 1 V and 5.1 V in order to extract at least one lithium.

4. Conclusion

The new compound $Li_{1.65}Na_{0.35}Fe[PO_4]F$, prepared from the analogous $LiNaFe[PO_4]F$ phase by ion exchange using LiBr in ethanol at 90°, is isostructural to $Li_2Ni[PO_4]F$. The combination of X-ray diffraction, EDX, and ICP analyses indicates the presence of Li/Na disorder at the 8*d* position, suggesting that the ion exchange was not total after 48 h. Furthermore, the Mössbauer analyses indicates that the chemical composition is rather $Li_{1.65}Na_{0.35}[Fe^{2+}{}_{1-x}Fe^{3+}{}_x][PO_4][F_{1-x}O_x]$ ($x \sim 1/4$) than $Li_{1.65}Na_{0.35}Fe[PO_4]F$. The electrochemical tests indicate that Li/Na ion exchange occurs during cycling which leads to a lithium rich phase $Li_{2+x}Fe[PO_4][F_{1-x}O_x]$ ($x \sim 1/4$). When cycled between 1.0 V and 5.1 V *vs.* Li^+/Li, only 1 mol of alkali metal is extractable, with a discharge capacity between 135 and 145 mAh g^{-1}. The doping of $LiNaFe[PO_4]F$ with manganese did not allow the extraction of the second lithium atom, but a severe decrease of the electrochemical performances as observed in the pyrophosphate compounds $Li_2Fe_{1-x}Mn_xP_2O_7$ [21,22].

Acknowledgments

Part of this work was carried out in the Li-EAD Project of the New Energy and Industrial Technology Development Organization (NEDO) in Japan.

Appendix A. Supplementary data

Supplementary data related to this article can be found at http://dx.doi.org/10.1016/j.jpowsour.2013.03.128.

References

[1] M.S. Whittingham, Chem. Rev. 104 (2004) 4271.
[2] J.M. Tarascon, M. Armand, Nature 414 (2001) 359.
[3] W.J. Zhang, J. Power Sources 196 (2011) 2962.
[4] Z.L. Gong, Y.X. Li, G.N. He, J. Li, Y. Yang, Electrochem. Solid-State Lett. 11 (2008) A60.
[5] S. Okada, M. Ueno, Y. Uebou, J.I. Yamaki, J. Power Sources 146 (2005) 565.
[6] M. Nagahama, N. Hasegawa, S. Okada, J. Electrochem. Soc. 157 (6) (2010) A748.
[7] T.N. Ramesh, Kyu Tae Lee, B.L. Ellis, L.F. Nazar, Electrochem. Solid-State Lett. 13 (4) (2010) A43.
[8] X. Wu, J. Zheng, Z. Gong, Y. Yang, J. Mater. Chem. 21 (2011) 18630.
[9] B.L. Ellis, W.R.M. Makahnouk, Y. Makimura, K. Toghill, L.F. Nazar, Nat. Mater. 6 (2007) 749.
[10] B.L. Ellis, W.R.M. Makahnouk, W.N.R. Weetaluktuk, D.H. Ryan, L.F. Nazar, Chem. Mater. 22 (2010) 1059.
[11] H. Ben Yahia, M. Shikano, K. Tatsumi, S. Koike, H. Kobayashi, Dalton Trans. 41 (2012) 5838.
[12] H. Ben Yahia, M. Shikano, S. Koike, K. Tatsumi, H. Kobayashi, H. Kawaji, M. Avdeev, W. Miiller, C.D. Ling, J. Liu, M.-H. Whangbo, Inorg. Chem. 51 (2012) 8729.
[13] H. Ben Yahia, M. Shikano, H. Sakaebe, S. Koike, M. Tabuchi, H. Kobayashi, H. Kawaji, M. Avdeev, W. Miiller, C.D. Ling, Dalton Trans. 41 (2012) 11692.
[14] V. Petricek, M. Dusek, L. Palatinus, JANA2006, Structure Determination Software Programs, Institute of Physics, University of Prague, Prague (Czech Republic), 2006.
[15] M. Dutreilh, C. Chevalier, M. El-Ghozzi, D. Avignant, J.M. Montel, J. Solid State Chem. 142 (1999) 1.
[16] I.D. Brown, D. Altermatt, Acta Crystallogr. B41 (1985) 244.
[17] N.E. Brese, M. O'Keefe, Acta Crystallogr. B47 (1991) 192.
[18] C. Vidal-Abarca, P. Lavela, J.L. Tirado, A.V. Chadwick, M. Alfredsson, E. Kelder, J. Power Sources 197 (2012) 314.
[19] N. Marx, L. Croguennec, D. Carlier, A. Wattiaux, F. Le Cras, E. Suard, C. Delmas, Dalton Trans. 39 (2010) 5108.
[20] A.M. Sukeshini, H. Kobayashi, M. Tabuchi, H. Kageyama, Solid State Ionics 128 (2000) 33.
[21] H. Ben Yahia, M. Shikano, H. Kobayashi. Mater. Chem. Phys., submitted.
[22] H. Zhou, S. Upreti, N.A. Chernova, G. Hautier, G. Ceder, M.S. Whittingham, Chem. Mater. 23 (2) (2011) 293.